

# **Dynamic Resolution Control in a Laser Projection based Stereolithography System**

Yayue Pan\*, Chintan Dagli

Department of Mechanical and Industrial Engineering, University of Illinois at Chicago, Chicago, IL 60607

\* Corresponding author: [yayuepan@uic.edu](mailto:yayuepan@uic.edu), (312)996-8777

REVIEWED

## **Abstract**

In a typical Additive Manufacturing system, it is critical to make a trade-off between the resolution and build area for applications in which varied dimensional sizes, feature sizes, and accuracies are desired. The lack of the capability in adjusting resolution dynamically during building processes limits the use of AM in fabricating complex structures with big layer areas and small features. In this paper, a novel AM system with dynamic resolution control by integrating a laser projection in vat photopolymerization process is presented. Theoretical models and parameter characterizations are presented for the developed AM system. Accordingly, the process planning and mask image planning approaches for fabricating models with varied dimensional sizes and feature sizes have been developed. Multiple test cases based on various types of structures have been performed.

**Keywords:** Additive Manufacturing, vat photopolymerization, Stereolithography, Resolution Control, Build Size

## **1. Introduction**

### **1.1 Backgrounds and motivations**

Additive Manufacturing (AM), often referred to as Solid Freeform Fabrication (SFF) or 3D Printing or Rapid Prototyping, is a class of technologies that can fabricate parts with almost any freeform geometries directly from three-dimensional computer aided models by accumulating material together, usually in a layer by layer manner.

In past decades, intensive research attempts have been made to improve the performance of AM systems, in terms of build speed [1, 2], surface quality [3-5], material property[6-8], process reliability [7], etc. This technology finds its applications as a rapid prototyping technology in a wide variety of fields such as architecture, construction, industrial design, automotive, aerospace, military, engineering, medical, biotech, fashion, footwear, jewelry and education [9-11]. However, many limitations still exist in AM and hinder its application in fabricating end-use products, including size and resolution limitations, imperfections, limited choices of materials, low through-put, etc. [12]. In this research, we focus on working to overcome one of its primary

drawbacks: size and resolution limitations, in a Stereolithography related AM system which has entered the mainstream of 3D printing industry.

Stereolithography (SL) related AM technology can achieve a wide range of resolutions. As of today, various commercial machines have successfully entered the market, typically offering resolutions in the range of  $20\mu\text{m} \sim 200\mu\text{m}$  and build envelope diagonal size of  $30 \sim 500$  mm. There are two types of Stereolithography related AM technologies: laser scanning based, and projection based technologies. In the early stage, laser beam is used in SL system to cure liquid resin path by path to form one layer. With the advancement in Micro-Electro-Mechanical Systems (MEMS), projection based SL process becomes a more popular SL related AM technology these years due to their dynamic mask generation capability. In a projection SL system, a digital micromirror device (DMD) is usually used to pattern the light. A DMD is a Micro-Electro-Mechanical Systems device that enables one to simultaneously control small mirrors that turn on or off a pixel at over 5 KHz. Using this technology, a light projection device can project a dynamically defined mask image onto a resin surface to selectively cure liquid resin into layers of the object. Consequently, the related AM process, Mask Image Projection Stereolithography (MIP-SL), can be much faster than the laser based SL process by simultaneously forming the shape of a whole layer, and can achieve a much higher resolution by having a big number of micro-mirrors and focusing each pixel in a small area. Many research groups demonstrated micro-manufacturing capability with micron or even sub-micron scale resolution in MIP-SL systems [3, 5, 13-15].

Despite the advancement of SL related AM technologies, conflict between the build size and resolution is a historically inherent manufacturing dilemma. In order to achieve higher resolution, a smaller laser beam spot or a smaller pixel size is desired, in turn, a smaller build size will be created. Due to the fundamental energy distribution mechanism in SL related AM technologies, build size and resolution have always been two conflicting goals. Recently a method to solve this dilemma by projecting multiple images in different areas to make one big layer is proposed by Emami et. al [16]. However this approach will lengthen the build time greatly and make the process much more complicated.

The thrust of this research is to contribute to the advancement of AM by addressing such a dilemma of the resolution and build size, without affecting other manufacturing performance factors like build speed and process reliability. To achieve this goal, a continuous resolution control approach is investigated by using a laser projection technology.

## 1.2 Novelty and Contributions

A schematic diagram of the conventional MIP-SL process is represented in Fig. 1a. A lamp is usually used as a light source and a DMD chip is used to pattern the light. Optical lens is used to focus the patterned light onto a liquid resin surface. In a system, the resolution is determined by the lens' focal length and fixed. To cure a layer with different area, different number of pixels

could be illuminated. As shown in Fig. 1b, with the conventional approach, the curing area of a layer could be adjusted along a line segment by adjusting the number of illuminated pixels. For example, assume there are  $1024 \times 768$  pixels in total and the pixel size is  $r_2$ , the curing area that could be adjusted by changing the number of illuminated pixels and the control freedom is the green line segment. In order to enlarge the build volume, the pixel size  $r_2$  should be increased which in turn will reduce the achievable resolution, causing the dilemma between resolution and build size.

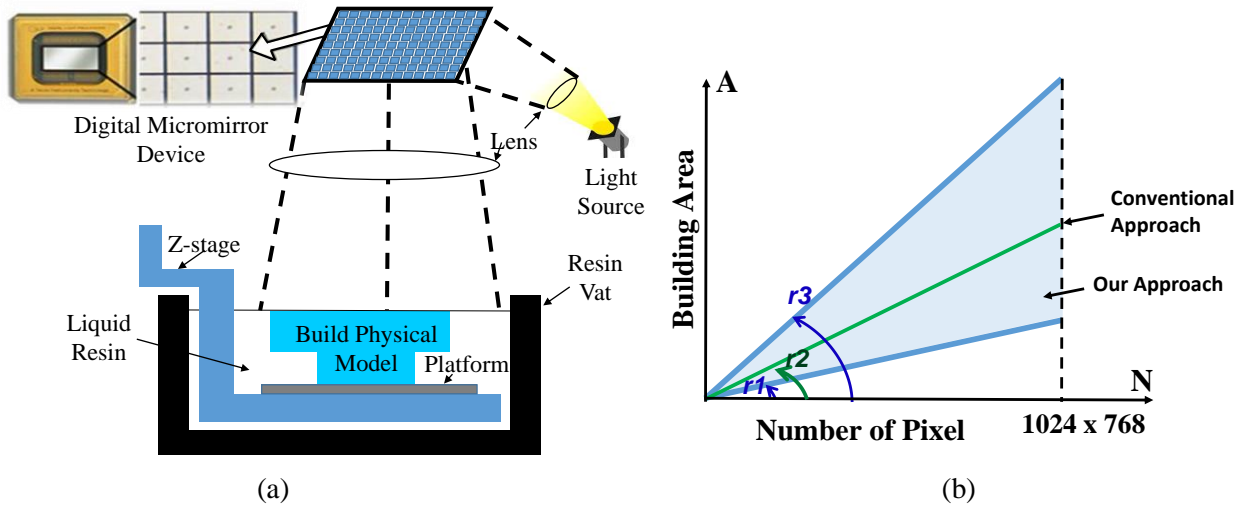


Figure 1. (a) Schematic illustration of conventional MIP-SL systems (b) Pixel number- Curing area relation in conventional approach and our approach

To address this problem, we propose a dynamic and continuous resolution control approach for MIP-SL systems. With our approach, the pixel size can be adjusted dynamically within a certain range from  $r_1$  to  $r_3$ . Consequently, the control freedom is a 2-D area, instead of a 1-D line segment, as the light blue area showed in Fig 1b.

This novel dynamic resolution control approach is presented in the following sections. Section 2 presents an overview of a novel Laser-Projection based Stereolithography (SL) System with the resolution control approach along with its flowchart explaining the working of the system. A special Mask Image Processing Algorithm for dynamic resolution control is presented in Section 3, followed with a parametric dependence quantification process investigated in Section 4. Multiple test cases are demonstrated and discussed in Section 5. It is shown that parts with varying layer sizes and feature sizes could be fabricated with desired resolutions, by using this approach. Finally, conclusions are made in Section 6.

## 2. Overview of the Laser Projection based SL System

Instead of a lamp, a laser is used as a projection light source in our system. The laser projector has unique properties including focus free operation, capability to produce dynamic mask image irrespective of any surface (flat or curved) as shown in Fig. 2. And last but not the least is its

compact size that makes it easy to be adopted and integrated into the additive manufacturing system. These unique characteristics of laser projector eventually provide a distinct capability to change the projection image size and resolution easily.

The laser projector is composed of three LEDs (blue, red and green) and a MEMS scanner. The projected image is created by modulating the three lasers synchronously with the position of the scanned beam [17]. The projected beam directly leaves the MEMS scanner and creates a sharp image irrespective of any surface (flat or curved) it is shone upon [17].



Figure 2. Laser Projector unique properties: (a) Stays focus when changing focal length; (b) Project on any shape surface

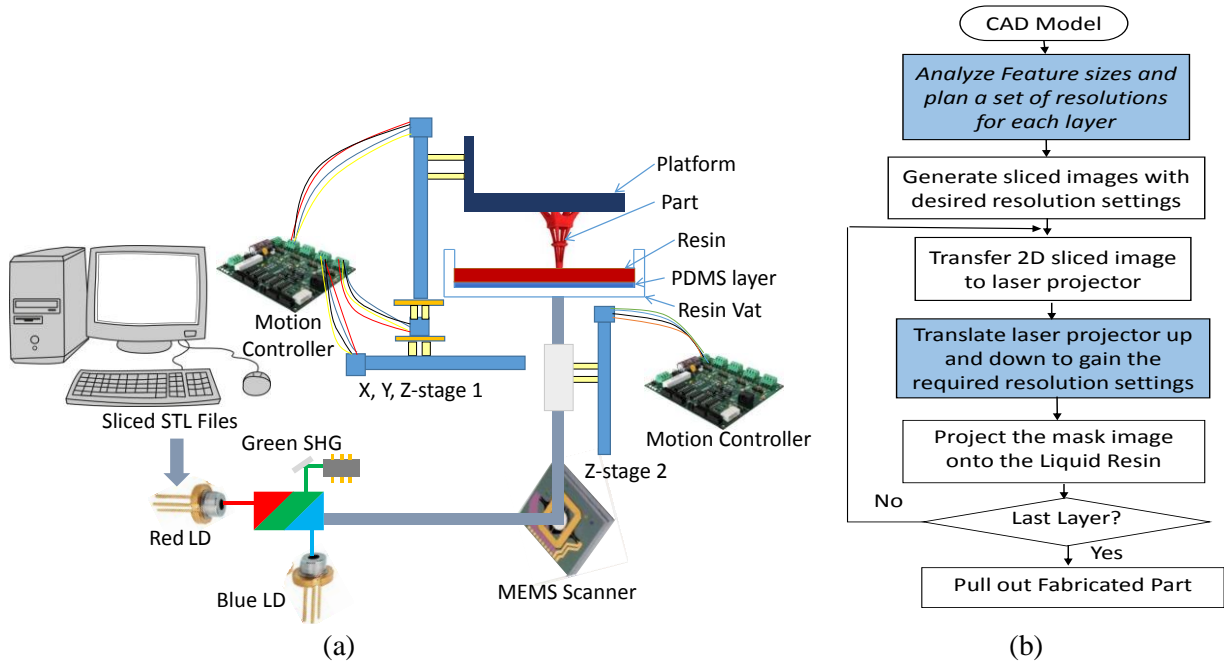


Figure 3. (a) A Laser Projection based SL system with dynamic resolution control (b) Flowchart of the working of Laser Projection based SL system

The Laser Projection based SL system design is shown in Fig. 3a above and the flowchart in Fig. 3b explains the working of the entire system. Similar to the conventional approach, we start from a CAD model. However, instead of slicing the STL file with a certain predefined resolution setting, we first analyze feature sizes of the CAD model, and then set a resolution for each layer. After that, mask images will be generated by slicing each layer with the desired resolution setting. These mask images are then transferred to the laser projector for layer by layer fabrication. The laser projector then moves to a corresponding position to cure that layer with the

desired resolution and simultaneously the pixel size changes dynamically according to the position of laser projector. Therefore, in this dynamic resolution control manufacturing process the above two steps highlighted in blue are the most important. Correspondingly, two fundamental research questions need to be answered:

1. How to determine a proper set of resolutions for each layer to achieve best part quality.
2. How to move projector to the proper position to gain the required resolution.

Question 1 will be answered in Section 3 by exploring an image processing algorithm to filter features with different resolution requirements. Question 2 will be investigated in Section 4 by quantifying the parametric dependence of resolution and build size on manufacturing process parameters.

### **3. Image Processing Algorithm**

It is therefore very essential to answer the first question about how to determine proper resolution for each layer so as to obtain best quality part and therefore we proposed an image processing algorithm to answer this question. For instance, a solid freeform fabrication design model is sliced into a set of layers and it might have micro-scale and a macro-scale features in a single layer. If this layer is fabricated with a proper resolution corresponding to the macro-scale feature, the micro feature could not be fabricated out due to the insufficient resolution. However, if a high resolution setting is used to give the required accuracy for fabricating micro features, the build size may not be big enough to fabricate out the whole layer. Therefore, for each sliced layer, a proper resolution or a proper set of resolutions need to be determined to achieve the desired accuracy and build size for that layer without sacrificing the other manufacturing performances like build speed.

In this study, a single Layered Depth Image (LDI) algorithm is utilized to determine the proper set of resolutions for each layer. LDI is generally used for 2-dimensional images which can be extended further to Layered Depth-Normal Images commonly known as LDNI [18]. In the following sections, for easy understanding, we use "micro feature" or "micro image" to denote an area which has to use a high resolution R1 to fabricate, and "macro feature" or "macro image" to denote an area which could use a low resolution R2 to fabricate.

The following example Fig. 4 illustrates a simple sliced binary image for a single layer that contains micro feature in a large area. We segmented the micro features from the macro part so as to build these small features with higher resolution in order to highlight its intricate details. Let V comprises of the entire image having i pixels along X-direction and j-pixels along Y-direction. Originally, the image is sliced by using the lowest resolution setting in our system, which is 81 microns per pixel denoted as R81. This can be represented as  $(X_i, Y_j) \in V$  for a single layer that can be extended to the 3<sup>rd</sup> dimension identifying the K<sup>th</sup> sliced layer. Thus the overall equation can be represented as  $(X_i, Y_j) \in V_{Layer\_K}$ . In order to filter the micro feature which cannot

be fabricated by using the lowest resolution R81, rays are transmitted along each row pixel first and then each column pixel. We consider each row as a separate image and run the loop. When the ray identifies a pixel that has its neighboring pixel of different intensity it shall be marked as the boundary of the object.

In the following example, a sectional part is highlighted to show the working of the algorithm. The system identifies the object pixel and mark the boundary pixel at the respective position as  $X_{i,n}$ , where n is the change in the pixel intensity ranges from 0 to infinity. The ray starts with n value as 0 and changes to 1 immediately when it finds the 1<sup>st</sup> boundary pixel and then proceeds with an increment when it encounters discontinuity. Thus, the next boundary will have  $X_{i+p,n+1}$ , where p is any arbitrary value of X position. The distance between any two boundaries of an object can be generalized as  $d|X_{i+p,n\_even} - X_{i,(n\_even)-1}|$ , except when n is 0. We set a threshold value T for the pixel distance which indicates that if the distance between two boundary object pixel exceeds the threshold it will be counted as meso-scale or macro-scale feature, whereas if the distance between the boundary object pixel is less than the threshold it will be counted as the micro-scale feature which cannot be fabricated by using resolution R81 and the object pixel will be marked as 0.

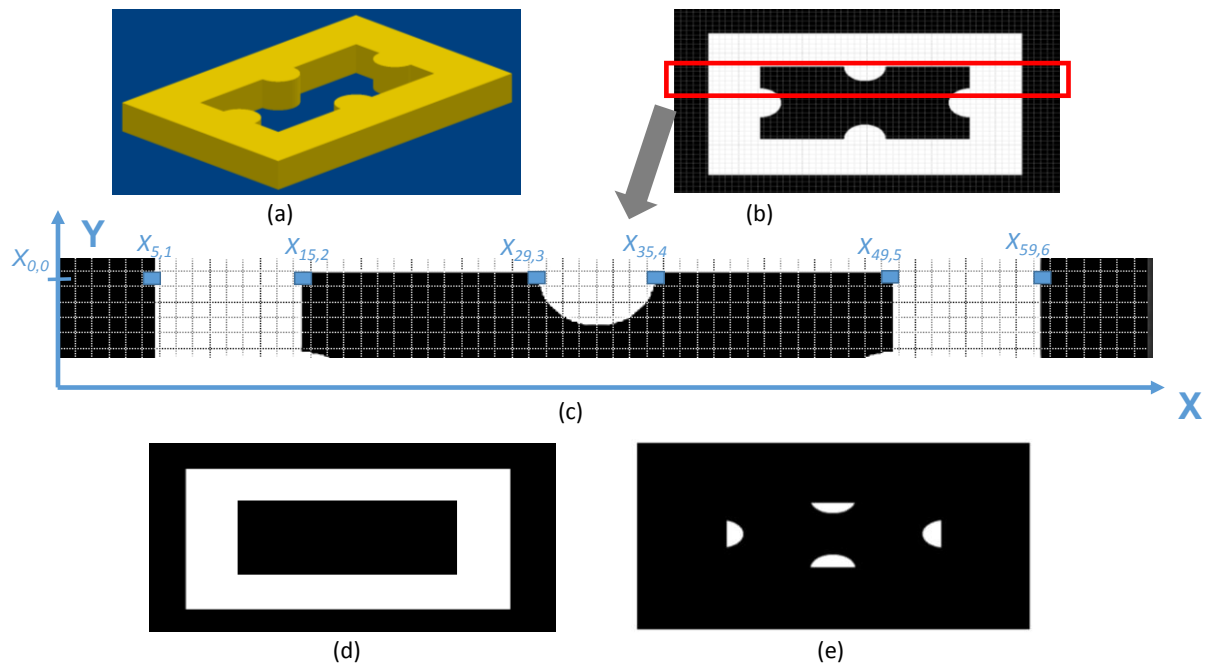


Figure 4. Example Model (a) STL Model; (b) Transfer Rays along Rows and Columns of a Binary Sliced Layered Image; (c) Sectional View highlighting object and boundary detection; (d) Macro Image; (e) Micro Image

For example, in the sectional image in Fig. 4, the ray transmitted along the row starts with n as 0 and then ends with n as 6, thus the row has 6 boundaries and 3 objects. It is identified that the  $d|X_{15,2} - X_{5,1}|$  and  $d|X_{59,6} - X_{49,5}|$  is greater than the threshold T, thus identified as macro image. On the contrary, the other object is micro image since the  $d|X_{35,4} - X_{29,3}|$  is less than T. After

identifying the micro-scale features, it will set all micro pixel object area to zero, we run the loop for all the rows and then a new image is generated. For better efficiency we then run this loop for all the columns on the new image and again the identified micro objects are set zero forming a modified image. The modified image thus obtained is the macro image and subtracting this modified image from the initial image will give out a micro image. Then the macro image is used for fabricating the related part by using R81. The micro features separated from the original sliced image, a higher resolution R81- $\Delta$  (denoting a resolution of 81- $\Delta$  microns per pixel) is used to regenerate an image for the micro features. Then the regenerated image is used as the input image and is processed the same way to determine a proper resolution for it. Following algorithm provides a throughout understanding of the working of image processing approach. R# means a resolution of # microns per pixel.

#### **Algorithm1:**

##### **INPUT**

A binary image sliced by using R#, V of K<sup>th</sup> layer.

##### **OUTPUT**

1. Macro Image
2. Micro Image

##### **STEPS**

1. Transfer rays from Y<sub>j</sub> till Y<sub>j+w</sub>, where j=0 → w and w = number of pixels along Y-axis
2. For each row find boundary pixel, X<sub>i,n</sub>, where i=0 → v and v= number of pixels along X-axis and n= change in pixel intensity
3. If  $d|X_{i+p,n\_even} - X_{i,(n\_even)-1}| \geq T$ , macro image else micro-image
4. If  $d|X_{i+p,n\_even} - X_{i,(n\_even)-1}| < T$ , set  $d|X_{i+p,n\_even} - X_{i,(n\_even)-1}| = 0$
5. New image as V\_row
6. Repeat above steps for column rays on V\_row
7. Store the modified image V\_mac
8. V\_mic = V - V\_mac

##### **RESULT**

V\_mac as macro image which will be used to fabricate a part of that layer using resolution R#  
V\_mic as micro image which the resolution needs to be updated.

#### **4. Parametric Dependence Quantification**

After obtaining the desired resolutions for each layer using Image Processing Algorithm, the next thing is to move the laser projector to the corresponding position to fabricate that part of that layer with its desired resolution. This is quantified by the dependence of pixel size and build size on the focal length. By moving the laser projector up and down using Z-stage 2 as shown in Fig. 3a, the digital mask images exposed on the liquid resin would have changing resolution and build size. More specifically if the laser projector is moved away from the platform the pixel size increases which means lower resolution but bigger build area. For example, the micro scale

structures could be segmented and fabricated with a small focal length and hence higher resolution, while the meso-scale structures in the model could be fabricated with a bigger focal length and hence larger curing area. The following section shows the relationship between pixel size and build size on the focal length.

#### **4.1 Quantifying Parametric Dependence of: Build Area & Resolution on Focal Length**

Due to the laser property of producing focus free masks irrespective of any focal distance, it provides a wide variety of resolution depending upon its distance from the bottom surface of resin vat. Thus, a process planning approach is essential for determining the position of the projector to obtain the required resolution for each layer. Both the resolution and building area are related to the focal length and there exist a linear co-relationship which has been highlighted in the following Fig. 5. The graph highlighted in red is related to the focal length and the resolution (y-axis on the right termed as  $y_2$ ) it produces whereas the graphs in blue (dashed line) and orange (round dotted line) are associated to the focal length and building sizes (y axis on the left termed as  $y_1$ ) along X and Y-axis respectively. The linear relationship between focal length  $x$  and building area  $y$  could be formulated as the following:

$$y_1 = 0.8 * x + 14.1333 \quad \text{along X-axis}$$

$$y_1 = 0.8 * x + 14.1333 \quad \text{along Y-axis}$$

whereas, Focal Length  $x$  (mm) and Planar Resolution  $y$  (micron/pixel) could be described by:

$$y_2 = 0.9906 * x + 16.6597$$

From the above equations, it's obvious that for producing parts with high resolution the focal distance between the laser projector and resin vat should be small and conversely for the development of parts with large area its focal distance will be large. Given a desired resolution, the projector could be moved to the corresponding position. Also, the fabrication of one layer with large area but small features, the mask image could be segmented into multiple images for multiple curing with different projector positions. As shown in Fig. 5, the projector provides a good flexibility with a building area of 73.0 mm to 31.0 mm along X-axis and 41.32 mm to 17.54 mm along Y-axis subject to the focal length of 70.0 mm to 20.0 mm respectively. Correspondingly, its resolution varies from 86.08 micron/pixel to 36.55 micron/pixel.

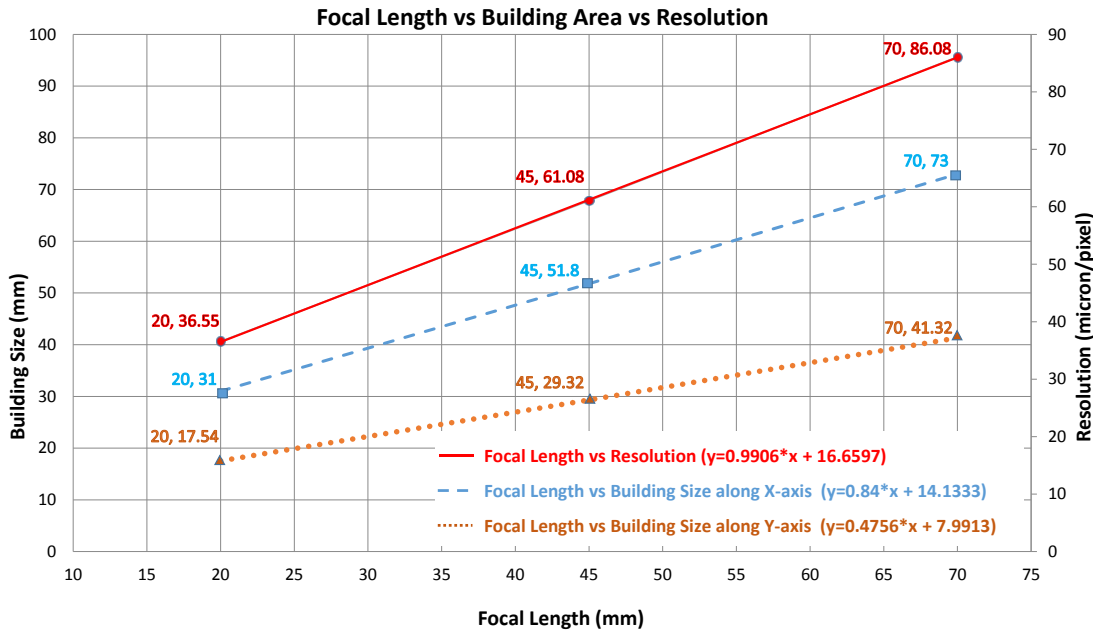


Figure 5. Graphical Relationship between Focal Length, Building Area and Planar Resolution

#### 4.2 Validating Beer Lambert Equation

To measure cure depth ( $C_d$ ) experiments were conducted for further analysis of the vertical resolution. The laser projector produced a mask at different focal lengths with each having a set of exposure time of 200 s, 300 s, 400 s, 500 s and 600 s. A commercial resin R5 red from Envisiontec containing 0.1-5% photoinitiator was utilized for the following set of experiments [19]. Other resin parameters such as penetration depth  $D_p$  and critical exposure  $E_c$  can be obtained from the Beer-Lambert formula provided in equation below [20].

$$C_d = D_p * \ln\left(\frac{E_{max}}{E_c}\right) \dots\dots\dots (1)$$

Also, the values of  $D_p$  and  $E_c$  can be verified from the graph below. The graph shows the relation between cure depth and exposure energy per unit area on the resin surface. The results indicate the cure depth is linearly proportional to the natural logarithm of the energy per unit area. Theoretically, the slope of the line is its penetration depth  $D_p$  and  $E_c$  is the energy when cure depth is 0, but this does not indicate the gel point of the resin [21]. It is observed from the graph that the value of  $D_p$  is 0.266 mm whereas  $E_c$  is 23.46 mJ/cm<sup>2</sup>.

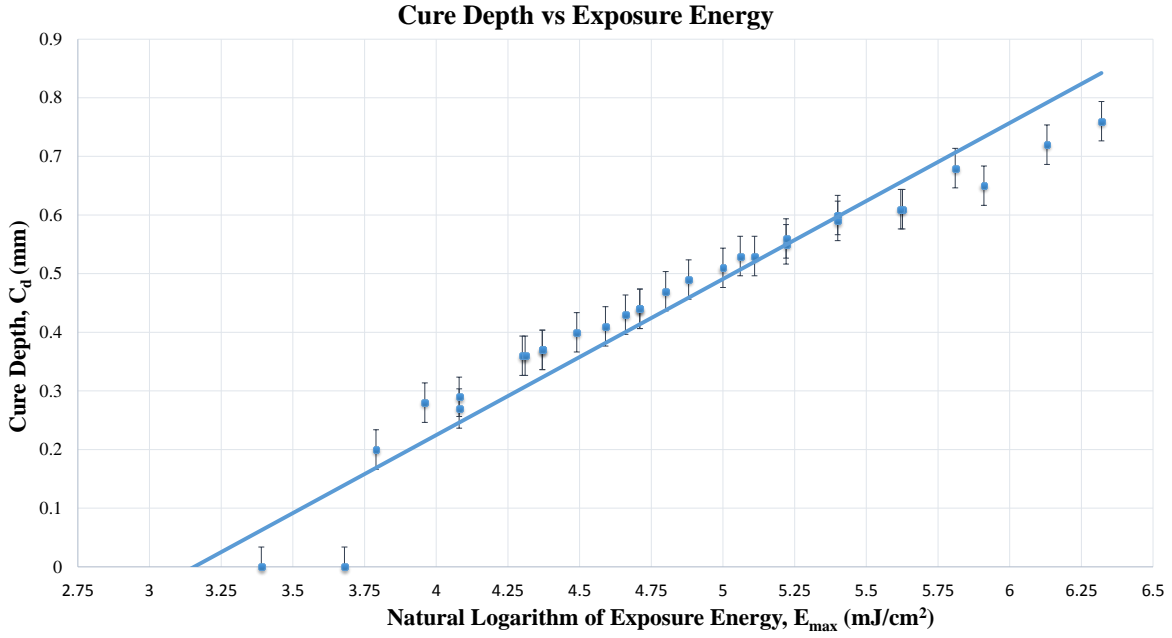


Figure 6. Graphical Relationship between Exposure Energy and Cure Depth

#### 4.2.1 Dependence of Cure Depth on Focal Length

On further extending Beer Lambert equation the relationship between the cure depth and focal length has been established using equation 1, as represented below:

$$C_d = D_p * \ln \left( \frac{E_{max}}{E_c} \right)$$

$$C_d = D_p * \ln \left( \frac{P_{max} * T}{A * E_c} \right) \dots\dots\dots (2)$$

where, P<sub>max</sub> = Laser Power, T= time, A= cured area.

Since all the variables in equation 2 are constant for a specific time and also the cured area is directly proportional to the focal length d, the above equation can be represented as follows:

$$C_d = D_p * \ln \left( \frac{K_{constant}}{d} \right)$$

$$C_d = D_p * \ln(K_{constant}) - D_p * \ln(d)$$

$$C_d = K'_{constant} - D_p * \ln(d) \dots\dots\dots (3)$$

Equation 3 can be validated with the graph below that justifies the relation between cure depth and focal length. These linear equations in Fig. 7 are obtained when the laser projector produce slice image on the build surface for a specified time under different focal length.

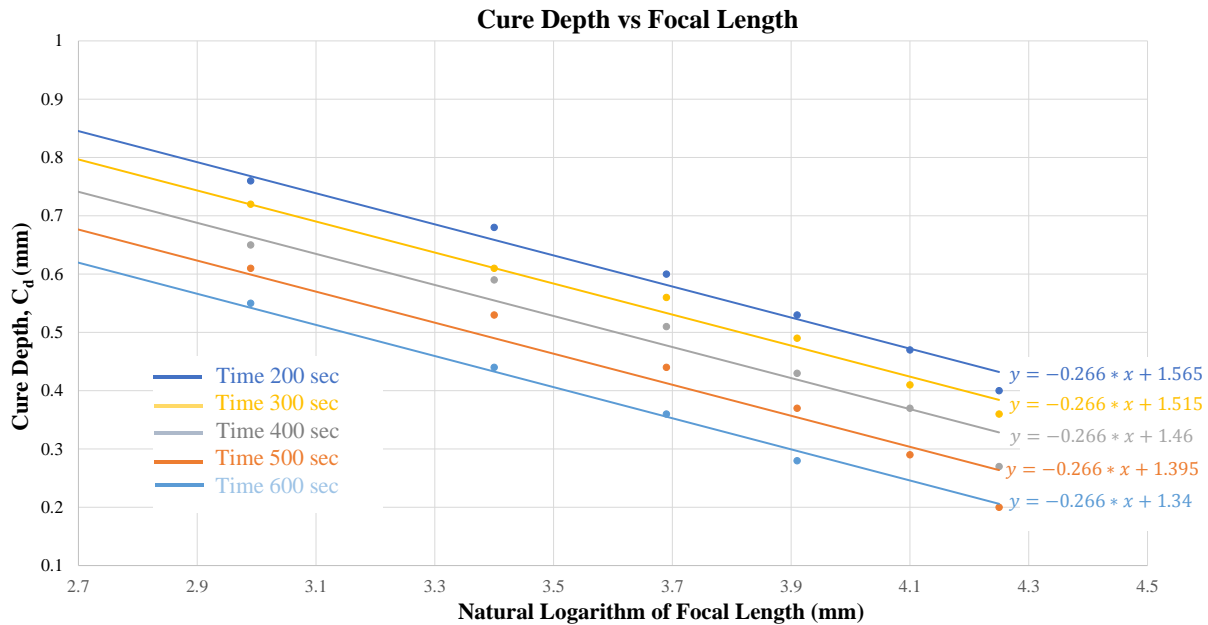


Figure 7. Graphical Relationship between Focal Length and Cure Depth

## 5. Experimental Results and Discussion

To validate the efficacy of the approach a testbed was developed and models with multiple resolutions, varied dimensional sizes were fabricated. These 3D STL models were initially sliced layer by layer into 2D images and projected through a portable laser projector. The unique feature of these experiments was providing dynamic motion to the laser projector during building process. This resulted in providing flexibility to fabricate parts with changing resolution in a single building task.

### 5.1 Large Area Fabrication Capability

The manufacturing capability of fabricating parts with large layer areas was tested and verified by fabricating a spur gear. The CAD model and fabricated result are shown in Fig. 8. After analyzing this model using our image processing algorithm it was found that the part can be fabricated with one resolution. A resolution of 81 micron/pixel was adopted which is good enough to produce all details of this gear model. Based on the resolution the laser projector's focal length was kept 65 mm so as to obtain the desired resolution.

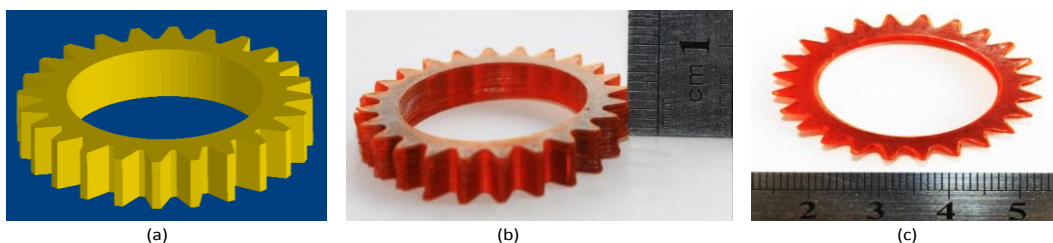


Figure 8. Gear:- (a) Isometric view of STL Model; (b) Isometric view of Built Part; (c) Top View of Built Part

This fabricated model constituted of 50 layers in total, including 7 base layers with a layer thickness of 90 microns. Initial exposure time for the base layer was 600 seconds per layer whereas for the subsequent layer it was 70 seconds each.

## 5.2 Small Area Fabrication Capability

The system showed appropriate results for large area fabrication. The same experimental setup was adopted to test the limits of resolution and fabricated parts with the small area. Also, to further endorse the system capability, minute details were added in the part. The CAD model as demonstrated in Fig. 9a is a hollow ball with nine circular cuts on its circumference. Four symmetric bigger circular cuts along the center whereas slightly above it includes four circular cuts of slightly smaller diameter. Lastly, the top portion is drilled to form a small circle. The image processing analysis showed that a single resolution, 30 micron/pixel works for fabricating the whole part with desired accuracy while a shortest build time. Thus, the focal length was fixed at 13.5 mm to give a 30 um/pixel resolution for building all layers.

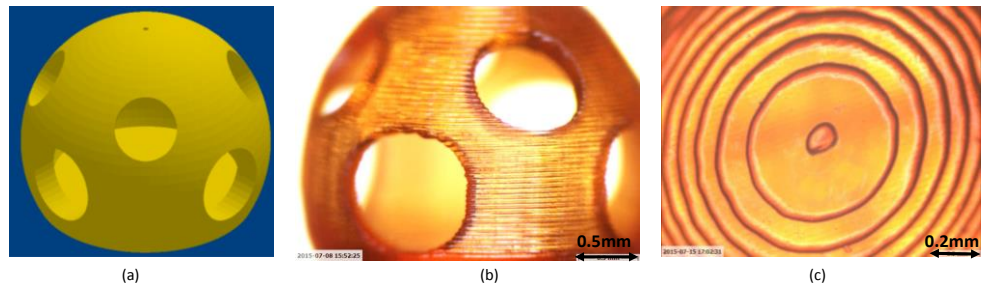


Figure 9. Hollow Ball; (a) Isometric view of STL Model; (b) Microscopic imaging of Isometric view of Built Part; (c) Microscopic imaging of Top view of Built Part

The fabricated part, thus formed was 2.8 mm in diameter and 2.65 mm in height with bigger and smaller circular cuts of diameter 800  $\mu\text{m}$  and 600  $\mu\text{m}$  respectively. Also, the top circular portion had a diameter of 70  $\mu\text{m}$ . The Fig. 9b and 9c are microscopic images of the isometric and top view of the part respectively. The entire structure was comprised of 63 layers including 7 base layers. Each layer corresponds to a thickness of 43 microns. Due to the reduced focal length the initial exposure time and the exposure time for both base and subsequent layers were kept as low as possible mainly 200 seconds and 30 seconds respectively.

## 5.3 Multi-Scale Resolution Fabrication Capability

The system successfully fabricated parts with micro and macro scale features separately. The following test case is conducted to verify the manufacturing capability of building multi scale features in a single building task. For this purpose a gear set with concentric center was designed as shown in Fig. 10a. With our dynamic resolution control method, after applying the image processing algorithm, we identified that for the bottom gear, a pixel size of 81 micron is good enough to give the desired accuracy and build size. Whereas for the top gear, since its feature is much smaller, a smaller pixel size, 41 micron is desired to fabricate the features precisely. After

setting up different resolutions for layers, we could assign the corresponding projector position. According to the parametric dependence developed in this research the focal length was obtained as 65 mm and 25 mm for the bottom and top gear respectively.

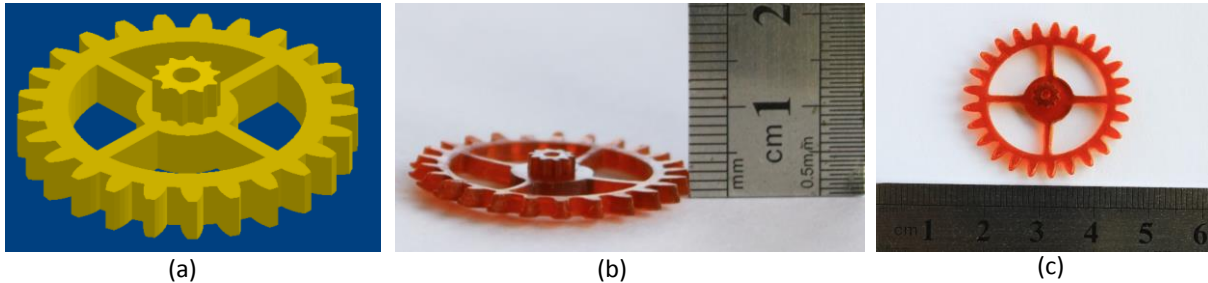


Figure 10. Multi-scale Gear; (a) Isometric view of STL Model; (b) Isometric view of Built Part; (c) Top view of Built Part

The fabricated part constituted 39 layers including 7 base layers with a layer thickness of 90 micron. The base layer were cured for 600 seconds whereas the subsequent layers were cured for 70 seconds. The bottom gear diameter comprised of 30.0 mm whereas the top gear diameter comprised of 5.00 mm with an overall depth of 3.8 mm.

#### 5.4 Continuous Resolution Control Fabrication Capability

The first two test cases in Section 5.1 and 5.2 demonstrate the capability of our approach on fabricating parts with different resolutions. Section 5.3 verifies the effectiveness and efficiency of our approach on fabricating a part with two different resolution settings in one build.

Furthermore, another test case is conducted to demonstrate the system capability in continuously changing the resolution for each layer. The STL file shown below in Fig. 11a consists of a triangular structure with a circular hole drilled through its center. Also, the two sides of the triangle are drafted by an angle of 55 degree. *Since the layer by layer sectional area of the part reduced continuously, the projector's focal length was also changed from 45.0 mm to 25.0 mm ultimately improving the resolution by 0.34 micron/pixel for each layer.* The projector's focal distance was controlled by synchronizing its motion with the platform.

The model comprised of 59 layers in total with each layer thickness corresponding to 76 micron. The base layer of the model was fabricated with a curing time of 300 seconds whereas the subsequent layers were cured for 30 seconds each. The isometric view along with part dimension is shown below in Fig. 11b and 11c. The side of the triangle is measured to be 18.0 mm whereas the circular hole has a diameter of 5.0 mm. The top tilted edge is 9mm long while the other two edges that correspond to the part thickness are measured to be 4.5 mm.

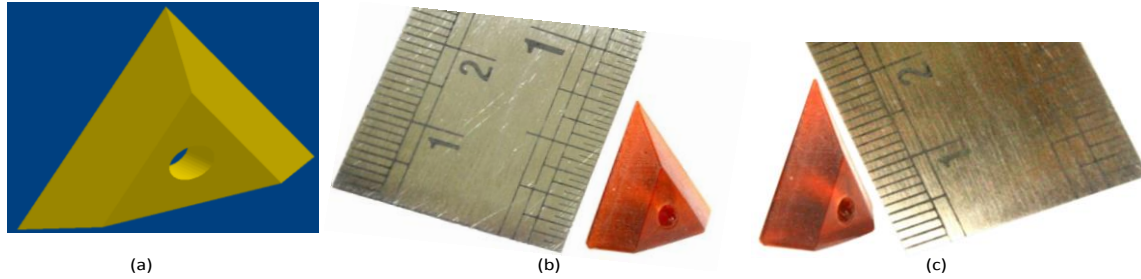


Figure 11. Titled Edges Triangular Surface; (a) Isometric View of STL Model; (b) Isometric View of Built Part with Side Measurement; (c) Isometric View of Built Part with Edge Measurement

## 5.5 Building Performance Statistics

The system demonstrated a unique characteristic of dynamic and continuously changing resolution. Also, the laser projector being so compact in size can be conveniently moved along the z stage without considering the factor of the getting a distorted image due to its focus free operation. To make a more straightforward comparison with conventional approaches, the building time for base layers is excluded in the part build time. The table below shows the capability of this approach on fabricating parts with different layer areas and feature sizes efficiently through changing resolutions dynamically and even continuously for each layer.

**Table 1. Statistics of all test cases**

	<b>Model 1 (Large Area)</b>	<b>Model 2 (Small Area)</b>	<b>Model 3 (Multi-scale)</b>	<b>Model 4 (Continuous resolution)</b>
<b>X-Y Dimension (mm)</b>	35.0 x 35.0	2.8 x 2.8	30.0 x 30.0 (big gear) 5.0 x 5.0 (small gear)	18.0 x 16.0
<b>Smallest feature (mm)</b>	~5	0.07	1	0.2
<b>Depth (mm)</b>	4.5	2.65	3.5	4.5
<b>Total number of Layers</b>	50	63	39	59
<b>Part Build Time (min)</b>	50	20	45	30
<b>Layer Thickness (microns)</b>	90	43	90	76

## 6. Conclusion

A novel mask image projection based stereolithography (MIP-SL) system has been developed to achieve dynamic resolution control. Compared to conventional MIP-SL systems, the light source in our design includes a compact laser projector that was mounted on a z-stage, which resulted in changing focal length and in turn projection area and resolution. To facilitate the mask image planning problem in dynamic resolution control approach, an image segmentation algorithm has been developed to separate micro features from a sliced image. Parametric dependence of resolution and build size on focal length have been calibrated and modeled. The

effectiveness and efficiency of the system has been verified with multiple test cases with various surface areas, feature sizes and structures.

## References

1. Ha, Y.M., et al., "Mass production of 3-D microstructures using projection microstereolithography" Journal of mechanical science and technology, 2008. 22(3): p. 514-521.
2. Pan, Y., et al., "A Fast Mask Projection Stereolithography Process for Fabricating Digital Models in Minutes" Journal of Manufacturing Science and Engineering-Transactions of the Asme, 2012. 134(5).
3. Pan, Y. and Y. Chen, "Smooth Surface Fabrication based on Controlled Meniscus and Cure Depth in Micro-Stereolithography" 2015.
4. Pan, Y., et al., "Smooth surface fabrication in mask projection based stereolithography" Journal of Manufacturing Processes, 2012. 14(4): p. 460-470.
5. Sun, C., et al., "Projection micro-stereolithography using digital micro-mirror dynamic mask" Sensors and Actuators a-Physical, 2005. 121(1): p. 113-120.
6. Pan, Y., et al., "Multitool and Multi-Axis Computer Numerically Controlled Accumulation for Fabricating Conformal Features on Curved Surfaces" Journal of Manufacturing Science and Engineering-Transactions of the Asme, 2014. 136(3).
7. Turner, B.N., R. Strong, and S.A. Gold, "A review of melt extrusion additive manufacturing processes: I. Process design and modeling" Rapid Prototyping Journal, 2014. 20(3): p. 192-204.
8. Zhao, X.J., et al., "An integrated CNC accumulation system for automatic building-around-inserts" Journal of Manufacturing Processes, 2013. 15(4): p. 432-443.
9. Brett P. Conner, et al., "Making sense of 3D printing: Creating a map of additive manufacturing products and services" Additive Manufacturing, Volume 1-4, October 2014, Page 64-76.
10. Klahn C., et al., "Laser additive manufacturing of gas permeable structures", Physics Procedia 41 (2013): 873-880.
11. Jane Chu, Sarah Engelbrecht, Gregory Graf, David W. Rosen, (2010) "A comparison of synthesis methods for cellular structures with application to additive manufacturing" Rapid Prototyping Journal, Vol. 16 Iss: 4, pp.275 – 283.
12. Huang, S.H., et al., "Additive manufacturing and its societal impact: a literature review" The International Journal of Advanced Manufacturing Technology, 2013. 67(5-8): p. 1191-1203.
13. Choi, J.-W., et al., "Fabrication of 3D biocompatible/biodegradable micro-scaffolds using dynamic mask projection microstereolithography" Journal of Materials Processing Technology, 2009. 209(15): p. 5494-5503.

14. Choi, J.W., et al., "Design of microstereolithography system based on dynamic image projection for fabrication of three-dimensional microstructures" Journal of mechanical science and technology, 2006. 20(12): p. 2094-2104.
15. Cheng, Y.-L. and M.-L. Lee, "Development of dynamic masking rapid prototyping system for application in tissue engineering" Rapid Prototyping Journal, 2009. 15(1): p. 29-41.
16. Emami, Mohammad Mahdi, Farshad Barazandeh, and Farrokh Yaghmaie. "Scanning-projection based stereolithography: Method and structure." Sensors and Actuators A: Physical 218 (2014): 116-124.
17. Microvision, Showmx Pico Projectors, [http://www.microvision.com/wp-content/uploads/2014/07/OPN\\_Article.pdf](http://www.microvision.com/wp-content/uploads/2014/07/OPN_Article.pdf)
18. Wang, C., and Chen, Y. "Layered depth-normal images: A sparse implicit representation of solid models" arXiv preprint arXiv:1009.0794 (2010).
19. Envisiontec Perfectly Material Data Sheet, <http://envisiontec.com/envisiontec/wp-content/uploads/MK-MTS-R5R11-V01-FN-EN.pdf>
20. Jacobs, Paul F., and David T. Reid. 1992. "Rapid prototyping & manufacturing: fundamentals of stereolithography" Dearborn, MI: Society of Manufacturing Engineers in cooperation with the Computer and Automated Systems Association of SME.
21. Gibson, Ian, David W. Rosen, and Brent Stucker, "Additive manufacturing technologies. New York: Springer" 2010.